Journal of Optoelectronics and Advanced Materials Vol. 1, No. 3, September 1999, p. 3 - 11

REVIEW PAPER

LIDAR: A POWERFUL TOOL FOR ATMOSPHERIC MEASUREMENTS

L. Fiorani

CORISTA, Piazzale Tecchio 80, 80125 Naples, Italy

Remote sensing systems are widely used to perform atmospheric studies. In particular, the optical radar or lidar has spread after the laser discovery. In this paper the lidar technique is introduced, three relevant applications are described (measurements of aerosols load, wind speed and pollutants concentration) and two typical experimental layouts are outlined. Finally, the advantages of the lidar with respect to usual techniques are discussed.

(Received August 26, 1999; accepted September 3, 1999)

Keywords: Remote sensing, Lidar, Atmosphere, Aerosols, Wind, Pollutants

1. Introduction

The aim of this paper is to introduce a reader familiar with optoelectronics to the lidar technique. A detailed description of all lidar applications will largely exceed the size at disposal. Anyway, some relevant atmospheric measurements will be discussed in order to illustrate the potential of such instrument.

The acronym "lidar" (Light Detection And Ranging) has been introduced in analogy with "radar" in the context of the pulsed light detectors of clouds [1]. Albeit this term has been suggested well before the discovery of the laser (conceived by Schawlow and Townes in December 1958 and realized by Maiman in July 1960) [2], only with its advent the lidar has spread.

The new capabilities offered to the atmospheric studies by this revolutionary source of light have been soon understood and exploited [3-6]. Because of its characteristics (high intensity, small divergence, short pulse duration and excellent monochromaticity) the laser beam is the ideal tool for active optical remote sensing. The measurement, up to many kilometers of height, of density, temperature and humidity of air, the detection of trace gases, the study of clouds, the observation of stratospheric aerosols, the probing of high atmosphere and the monitoring of pollutants are some examples among the possible applications of the lidar [7-10].

2. Lidar principle of operation

A lidar is essentially composed of a transmitter (laser) and a receiver (telescope). Its principle of operation is illustrated in Fig. 1: the backscatterers (molecules, aerosols) at the distance R from the system send back part of the laser pulse toward A, active surface of the telescope. Consequently, the analysis of the detected signal as a function of t, time interval between emission and detection, allows one to study the optical properties of the atmosphere along the beam, since the simple relation between t and R is given by:

$$R = \frac{ct}{2}, \tag{1}$$

where c is the speed of light.

The photons detected within τ_D, detector response time, are backscattered from the layer delimited by the distances R and $R+c\tau_D/2$. Their number n is proportional to the thickness $c\tau_D/2$ and to

the backscattering coefficient β of the involved air volume. Furthermore, in its round trip, the original pulse consisting of n_0 photons is attenuated by the atmosphere. This phenomenon is quantified by the extinction coefficient α. Moreover, n is proportional to the solid angle A/R^2 and the efficiency ζ of the detection system.

On the basis of the preceding discussion, the *lidar equation* can be finally written [8]:

$$n(R,\lambda) = n_0(\lambda)\zeta(\lambda)\frac{A}{R^2}\beta(R,\lambda)\frac{c\tau_D}{2}\exp\left[-2\int_0^R \alpha(R',\lambda)dR'\right]. \tag{2}$$

3. Measurement of aerosol load

The preceding section made clear that the lidar return is linked to the optical properties of the atmosphere along the laser beam. In general, the extinction and backscattering coefficient are determined mainly by the aerosol load. This parameter is important for its climatic effect, especially in Mediterranean towns [11]. Actually, α and β are both unknown, but some reliable methods have been elaborated to retrieve them from the signal, on the basis of some reasonable hypothesis [12-15]. In the following we will describe a scheme accepted by many researchers [16].

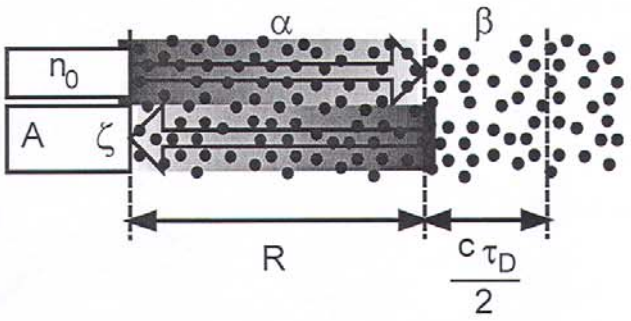

Fig. 1 Lidar principle of operation. The points represent generic atmospheric scatterers (molecules, aerosols).

As we have observed, at first glance equation (2) contains two unknown quantities: α and β. Moreover, it is often very difficult to establish precisely the efficiency of the system. Consequently, the retrieval of α and β requires not only to establish a relation between them, but also to estimate a constant. As we will see, this latter evaluation will be replaced by the determination of the backscattering coefficient at a given distance.

In order to establish a relation between the extinction and backscattering coefficients, we distinguish the contributions of molecules and aerosols:

$$\alpha(R,\lambda) = \alpha_r(R,\lambda) + \alpha_a(R,\lambda), \tag{3}$$

$$\beta(R,\lambda) = \beta_r(R,\lambda) + \beta_a(R,\lambda), \tag{4}$$

and we remember that the terms concerning molecular scattering (α_r and β_r) can be modeled very precisely [17,18]. Finally, we recognize that α_a and β_a are linked by the phase function P_π according to the equation:

$$\alpha_a(R,\lambda) = \frac{1}{P_\pi(R,\lambda)}\beta_a(R,\lambda). \tag{5}$$

Albeit the phase function varies with distance and time, in practice the final result is rather accurate even considering a constant P_π. The P_π value can be selected among those tabulated in the literature according to the aerosol kind (urban, rural, maritime etc.) [19].

After the definition [14]:

$$\mu(R,\lambda) \equiv \ln\left[n(R,\lambda)R^2\right] - 2\int_R^{R_M}\left\{\left[1-\frac{3}{8\pi P_\pi(R',\lambda)}\right]\alpha_r(R',\lambda)\right\}dR', \tag{6}$$

where R_M is a given distance, the following differential equation is obtained from relations (2) - (5):

$$\frac{d\mu(R,\lambda)}{dR} = \frac{1}{\beta(R,\lambda)}\frac{d\beta(R,\lambda)}{dR} - \frac{2}{P_\pi(R,\lambda)}\beta(R,\lambda), \tag{7}$$

whose solution is [12]:

$$\beta(R,\lambda) = \frac{\exp[\mu(R,\lambda)-\mu_M(\lambda)]}{\frac{1}{\beta_M(\lambda)} + \frac{2}{P_\pi(R,\lambda)}\int_R^{R_M}\exp[\mu(R',\lambda)-\mu_M(\lambda)]dR'}, \tag{8}$$

where:

$$\mu_M(\lambda) \equiv \mu(R_M,\lambda), \tag{9}$$

and β_M is the integration constant. Finally, from relations (3) - (5), we obtain the aerosols extinction and backscattering coefficients i.e. two parameters closely linked to the aerosol load. Solution (8) has been formulated so that β_M is equal to $\beta(R_M)$. If a large R_M is chosen (corresponding to the free troposphere), the aerosols contribution to the backscattering coefficient is negligible and then β_M can be computed very precisely.

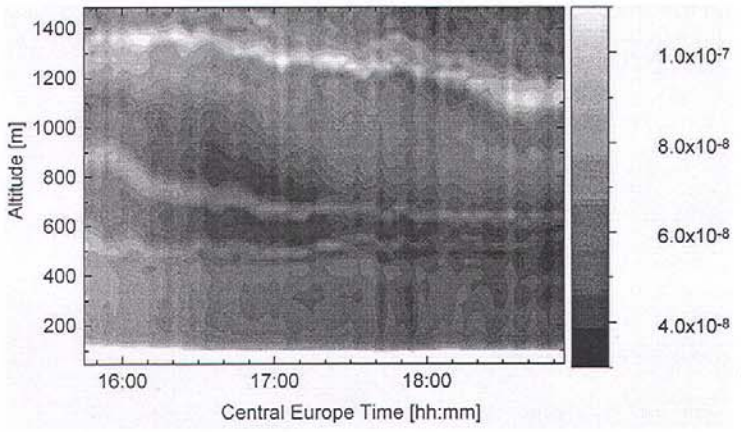

Fig. 2 Aerosol backscattering coefficient [cm^{-1} sr^{-1}] measured at 351 nm as a function of time and altitude (Naples, 13 March 1997).

Fig. 2 [20] is an example of the lidar capability to analyze the dynamics of the aerosol load in the low troposphere. At the beginning of the experiment four aerosol layers are clearly visible, one above the ground and three near 500, 900 and 1400 m of altitude. Note that around sunset (18:07 Central Europe Time) the convective activity diminishes, and consequently the upper layer bends down.

The analysis of the accuracy in the measurement of the aerosol extinction and backscattering coefficients is rather complex: we will summarize here only the main results, referring the reader to a specific study [21] for a more complete treatment. The statistical relative error of α and β is about equal to that of the lidar signal. This latter can be approximately written as [22,23]:

$$s_n = \sqrt{n + n_B + n_D}\ , \tag{10}$$

where n_B and n_D are the number of photon counts calculations originated by the brightness of the sky (solar background) and the electronic noise of the detector (dark current), respectively. The solar background can be computed from a model [24], the dark current is usually given by the manufacturer of the detector. Actually, equation (10) underestimates the statistical uncertainty, as it has been shown recently [25].

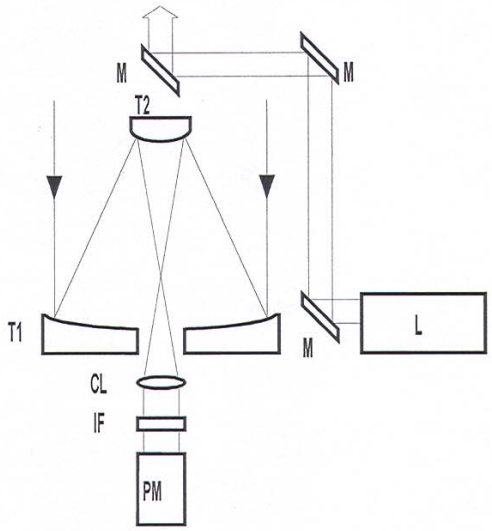

Fig. 3 Outline of a lidar conceived for the measurement of aerosols load.
L: laser, M: mirror, T1: telescope primary mirror, T2: telescope secondary mirror,
CL: collimating lens, IF: interference filter, PM: photomultiplier tube.

A typical layout of lidar conceived for the measurement of aerosol load is given in Fig. 3. It could be realized with commercial components and would be compact enough to be transported. The transmitter could be based on a Nd:YAG laser (1064 nm). This source has the advantage of being reliable and user-friendly. The receiver consists of a reflector telescope for light collection, of an interference filter for wavelength selection and of a photomultiplier tube (or an avalanche photodiode) for photon detection. The characteristics of the components listed in Table 1 are closely inspired to those of commercial models.

Table 1
Characteristics of a lidar conceived for the measurement of aerosol load.

Pulse energy [mJ]	400
Optical efficiency (transmitter and receiver) [%]	50
Photomultiplier quantum efficiency [%]	0.08
Filtering transmittance [%]	50
Filtering bandwidth [nm]	0.5
Photomultiplier dark current [counts per second]	7000
Telescope diameter [cm]	50

4. Measurement of wind speed

With minor modifications, the system just described can be used also for the measurement of wind speed. As we will see, all we need is the ability of steering the optics in any direction. In practice, the lidar can be aimed in two ways: either rotating together the transmitter-receiver couple or directing their optical axes by means of a pair of plain mirrors (like in an astronomic solar observatory).

According to equation (2), the number of photons backscattered by the atmosphere at a given distance from the instrument is proportional to the backscattering coefficient. This factor is a function of the density of aerosols responsible for the light scattering. Any change in its spatio-temporal distribution during a data acquisition will lead therefore to variations in the lidar returns from one laser shot to another. In particular, a wind flow along the beam axis will be detected from the transport of the spatial inhomogeneities of β along the optical path [26].

In order to simplify the formalism underlying the measurement of wind speed, let us consider a discrete distance variable: in the following an index i will be incremented over the spatial bins. First of all the signal is multiplied by the range squared and normalized by the emitted energy on a shot-per-shot basis, to define a normalized signal $S(R_i)$ independent of the energy fluctuation and proportional to the backscattering coefficient:

$$S(R_i) = n(R_i)\frac{R_i^{\,2}}{E_0} \tag{11}$$

The mean normalized signal $S'(R_i)$ is obtained by averaging N successively recorded individual signals at successive times t_n as:

$$S'(R_i) = \frac{1}{N}\sum_{n=1}^{N} S(R_i, t_n) \tag{12}$$

The information about the shot-per-shot fluctuations of the signals with respect to $S'(R_i)$ is contained in the fractional deviations:

$$f(R_i, t_n) = \frac{S(R_i, t_n) - S'(R_i)}{S'(R_i)} \tag{13}$$

In order to determine the displacement of the backscattering inhomogeneities, a cross-correlation function $\rho(L, z_a, z_b)$ is defined with respect to an altitude interval (z_a, z_b) and to a lag value L corresponding to a discrete number of spatial points as:

$$\rho(L, z_a, z_b) = \frac{1}{\sigma\sigma_L}\sum_{i=a}^{b}\sum_{n=1}^{N-1} f(R_i, t_n) f(R_{i+L}, t_{n+1}) \tag{14}$$

where:

$$\sigma^2 = \sum_{i=a}^{b}\sum_{n=1}^{N-1} f^2(R_i, t_n) \tag{15}$$

$$\sigma_L^2 = \sum_{i=a}^{b}\sum_{n=1}^{N-1} f^2(R_{i+L}, t_{n+1}) \tag{16}$$

$$z_i = R_i \sin\theta \tag{17}$$

$$\Delta R = R_{i+1} - R_i \tag{18}$$

$$\Delta t = t_{n+1} - t_n \tag{19}$$

where θ is the elevation angle of the telescope.

The radial wind speed v_R in the altitude interval (z_a, z_b) is determined from the lag value L_{max} for which the correlation is maximum:

$$v_R = L_{max}\frac{\Delta R}{\Delta t} \tag{20}$$

In the absence of vertical transport, the horizontal wind velocity is then estimated as:

$$v = v_R \cos\theta \cos\Phi \tag{21}$$

where Φ is the difference in the azimuthal orientation of the wind vector and of the light path.

An example of wind speed measurement is given in Fig. 4 [27].

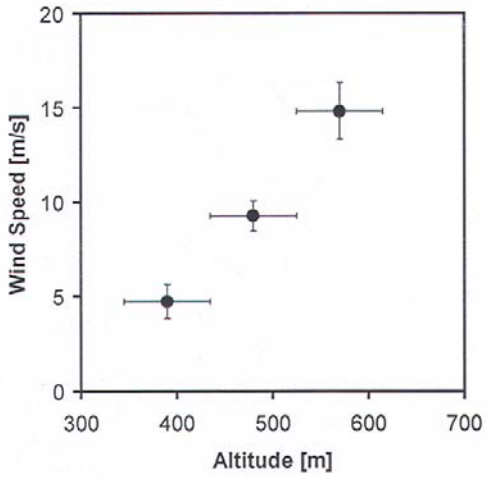

Fig. 4 Wind speed as a function of altitude (Athens, 13 September 1994).

5. Measurement of pollutant concentration

Laser remote sensing is widely used to measure pollutant concentration, usually by the differential absorption lidar (DIAL) technique [8]. This method is based on the detection of the backscattered photons from laser pulses transmitted to the atmosphere at two different wavelengths. At one wavelength (λ_{OFF}), the light is almost only scattered by air molecules and aerosols, whereas at the other one (λ_{ON}), it is also absorbed by the pollutant under study. The difference between the two recorded signals is thus related to the pollutant concentration. More precisely, on the basis of equation (2) the *DIAL equation* can be written [8]:

$$C(R) = \frac{1}{2[\sigma(\lambda_{ON}) - \sigma(\lambda_{OFF})]} \times$$
$$\times \left\{ \frac{d}{dR} \ln\left[\frac{n(R,\lambda_{OFF})}{n(R,\lambda_{ON})} \right] - \frac{d}{dR} \ln\left[\frac{\beta(R,\lambda_{OFF})}{\beta(R,\lambda_{ON})} \right] - 2[\alpha(R,\lambda_{ON}) - \alpha(R,\lambda_{OFF})] \right\}, \tag{22}$$

where $C(R)$ and $\sigma(\lambda)$ are, respectively, the concentration and the absorption cross-section of the pollutant molecule. If λ_{OFF} and λ_{ON} are close enough equation (22) gets simpler:

$$C(R) = \frac{1}{2[\sigma(\lambda_{ON}) - \sigma(\lambda_{OFF})]} \frac{d}{dR} \ln\left[\frac{n(R,\lambda_{OFF})}{n(R,\lambda_{ON})} \right]. \tag{23}$$

In both cases, the analysis of the accuracy in the measurement of the pollutant concentration is rather complex: once more the reader will find it elsewhere [21,28].

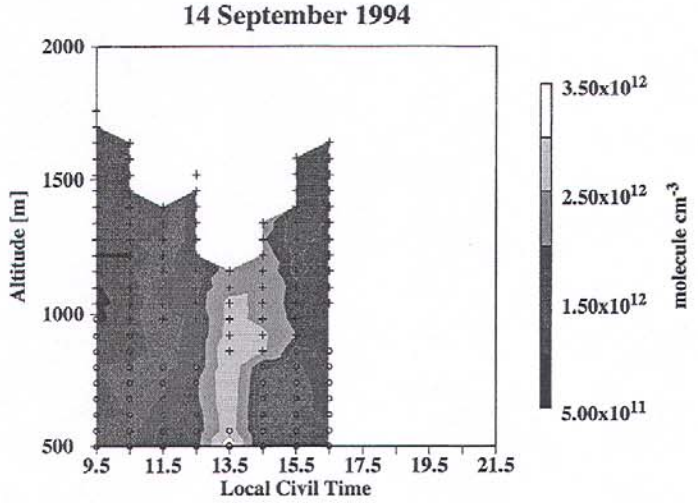

Fig. 5 Ozone concentration as a function of time and altitude (Athens, 14 September 1994).

Fig. 5 [29] is an example of ozone concentration measurement during a photochemical smog episode in Athens. Ozone concentration was successively increasing and decreasing during 14 September 1994, up to values as high as three times the background level during polluted days. This increase was responsible for a shortening of the measurement range due to a larger absorption of the emitted light. This effect was partially compensated for at 12:30 by a change of the experimental parameters inducing an increase of the SNR at a given altitude. However, this change was not sufficient to compensate for the important raise of the ozone concentration observed between 12:30 and 13:30. Consequently, the range at 13:30 was considerably lower than at 12:30. The photochemical smog episode was also visible from measurements performed with ground based punctual instruments installed near the lidar. The increase in ozone concentration was accompanied by a growth in the load of carbon black linked to a reduction of the visibility. These variations were due to a transport of pollutants from the center of the city to the site of measurement by a wind of about 0.8 ms^{-1} at the ground level blowing in that direction between 12:30 and 14:00. The wind direction then changes at 14:30, so that the pollutants are transported away from the site and the ozone concentration decreases down to its previous level.

Table 2
Characteristics of a lidar conceived for the measurement of pollutant concentration.

Pulse energy [mJ]	5
Optical efficiency (transmitter and receiver) [%]	50
Photomultiplier quantum efficiency [%]	25
Filtering transmittance [%]	50
Filtering bandwidth [nm]	2
Photomultiplier dark current [counts per second]	10
Telescope diameter [cm]	60

The layout of the system that performed the above-mentioned measurements is given in Fig. 6. A summary of its characteristics is given in Table 2. Two excimer pumped dye lasers equipped with frequency doubling crystals are used to generate λ_{ON} and λ_{OFF} (272.2 and 291.65 nm, respectively: these values represent a compromise between maximizing the difference in the ozone extinction coefficient, in order to improve the sensitivity of the measurement, and the necessity to minimize the corresponding difference in wavelength, as one wants to limit the uncertainties inherent in the correction for the differential extinction and backscattering by the aerosols; furthermore, they have been chosen so that there is no significant contribution of the SO_2 molecule to the differential absorption). Although the output energy from the XeCl excimer lasers reaches 400 mJ per pulse at a 100 Hz repetition rate, they are routinely set to provide about 300 mJ at 50 Hz for a better stability of the energy output over long periods of operation. Coumarin 153 and Rhodamine 6G are used for the generation of λ_{ON} and λ_{OFF} with a conversion efficiency near 15%. The throughput of the frequency doubling crystals is about 10%. The optical axes for the light emission and the light detection are separated by 430 mm in the apparatus. The geometrical position of the entry point of the emitted beam in the "cone" describing the volume of space "seen" by the detector defines an effective optical gate depending on the beam divergence and on the angle between the axis of the transmitter and of the receiver. At the exit of the Cassegrain telescope used for its collection, the light is injected through a lens into an optical fiber. The lidar returns are filtered by a spectrograph. An interference filter is placed after the slit selecting λ_{OFF} to further reject the solar background and to reduce the intensity of the signal to a value comparable to that obtained for λ_{ON}. Both signals illuminate approximately the same area of the active surface of a 12-stage photomultiplier tube. A normalization factor for the energy of each emitted light pulse is measured by integrating the current collected at the anode of a 5-stage photomultiplier tube. It is illuminated by less than 1% reflection off a plate. This reflection is attenuated by two neutral densities and one interference filter to avoid saturation.

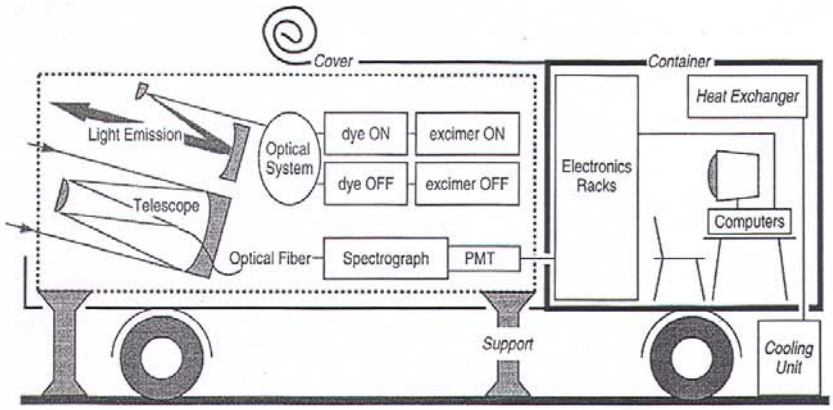

Fig. 6 Outline of a lidar conceived for the measurement of pollutant concentration.

6. Conclusion

During the second half of this century, the interest in environmental issues has steadily increased. In particular, many chemists, meteorologists and physicists have devoted their attention to the atmosphere. Range- and time-resolved measurements are necessary to study such a complex system. For this reason a large variety of instruments has been developed. Among them two important classes could be distinguished: "in situ" and remote sensors. The former have a long history and are often employed in routine applications for their reliable and simple operation. Among the latter, the lidar has spread after the laser discovery and presents many advantages with respect to usual techniques:

- continuous retrieval of aerosol load, wind speed and pollutant concentration profile in a considerable range and with a good spatio-temporal resolution;

- probe-less measurement, thus eliminating the possibility of modifying the sample;
- integrated-path determination, less sensitive to local effects;
- capability of sweeping the complete hemisphere, thus allowing to follow the physico-chemical dynamics of the atmosphere.

References

[1] Middleton W.E.K., Spilhaus A.F., Meteorological Instruments, University of Toronto, Toronto, 1953.
[2] Hecht J., Laser Pioneers, Academic Press, San Diego, 1985.
[3] Fiocco G., Smullin L.D., Nature **199**, 1275(1963).
[4] Goyer G.G., Watson R., Bull. Am. Meteorol. Soc. **44**, 564(1963).
[5] Collis R.T.H., Q. J. R. Meteorol. Soc. **92**, 220(1966).
[6] Derr V.E., Little C.G., Appl. Opt. **9**, 1976(1970).
[7] Collis R.T.H., Russel P.B., in Laser Monitoring of the Atmosphere, Ed. E.D. Hinkley, Springer-Verlag, Heidelberg, pag. 71, 1976.
[8] Measures R.M., Laser Remote Sensing, Krieger Publishing, Malabar, 1992.
[9] Clifford S.F., Kaimal J.C., Lataitis R.J. , Strauch R.G., Proc. IEEE **82**, 313(1994).
[10] Grant W.B., in Tunable Laser Applications, Ed. F.J. Duarte, Dekker Publishing, New York, pag. 213, 1995.
[11] Papayannis A., Balis D., Bais A., van den Bergh H., Calpini B., Durieux E., Fiorani L., Jaquet L., Ziomas I., Zerefos C.S., Atmos. Environ. **32**, 2193(1998).
[12] Klett J.D., Appl. Opt. **20**, 211(1981).
[13] Fernald F.G., Appl. Opt. **23**, 652(1984).
[14] Browell E.V., Ismail S., Shipley S.T., Appl. Opt. **24**, 2827(1985).
[15] Krichbaumer W., Werner C., Appl. Phys. B **59**, 517(1994).
[16] Durieux E., Fiorani L., in Instrument Development for Atmospheric Research and Monitoring, Eds. J. Bösenberg, D. Brassington, P.C. Simon, Springer-Verlag, Heidelberg, pag. 89, 1997.
[17] Elterman L., UV, Visible and IR Attenuation for Altitudes to 50 km – AFCRL-68-0153, United States Air Force, Hanscom, 1968.
[18] United States Standard Atmosphere, United States Government Printing Office, Washington, 1976.
[19] Shettle E.P., Fenn R.W., Models for the Aerosols of the Lower Atmosphere and the Effects of Humidity Variations on Their Optical Properties – AFGL-TR-79-0214, United States Air Force, Hanscom, 1979.
[20] Fiorani L., Armenante M., Capobianco R., Spinelli N., Wang X., Appl. Opt. **37**, 4758(1998).
[21] Fiorani L., Une Première Mesure Lidar Combinée d'Ozone et de Vent, à partir d'une Instrumentation et d'une Méthodologie Coup par Coup – Ph. D. Thesis 1985, École Polytechnique Fédérale de Lausanne, Lausanne, 1996 (in French).
[22] Schotland R.M., J. Appl. Meteor. **13**, 71(1974).
[23] Pelon J., Mégie G., J. Geophys. Res. **87**, 4947(1982).
[24] Kneizys F.X., Anderson G.P., Shettle E.P., Gallery W.O., Abreu L.W., Selby J.E.A., Chetwynd J.H., Clough S.A., Users Guide to LOWTRAN 7 – AFGL-TR-88-0177, United States Air Force, Hanscom, 1988.
[25] Durieux E., Fiorani L., Appl. Opt. **37**, 7128(1998).
[26] Eloranta E.W., King J.M., Weinman J.A., J. Appl. Meteor. **14**, 1485(1975).
[27] Fiorani L., Calpini B., Jaquet L., Van den Bergh H., Durieux E., Atmos. Environ. **32**, 2151(1998).
[28] Fiorani L., Calpini B., Jaquet L., Van den Bergh H., Durieux E., Appl. Opt. **36**, 6857(1997).
[29] Durieux E., Fiorani L., Calpini B., Flamm M., Jaquet L., Van den Bergh H., Atmos. Environ. **32**, 2141(1998).